

Unsupervised Radio Map Construction in Mixed LoS/NLoS Indoor Environments

Zheng Xing and Junting Chen

School of Science and Engineering (SSE) and Shenzhen Future Network of Intelligence Institute (FNii-Shenzhen)
The Chinese University of Hong Kong, Shenzhen, Guangdong 518172, China

Abstract—Radio maps are essential for enhancing wireless communications and localization. However, existing methods for constructing radio maps typically require costly calibration processes to collect location-labeled channel state information (CSI) datasets. This paper aims to recover the data collection trajectory directly from the channel propagation sequence, eliminating the need for location calibration. The key idea is to employ a hidden Markov model (HMM)-based framework to conditionally model the channel propagation matrix, while simultaneously modeling the location correlation in the trajectory. The primary challenges involve modeling the complex relationship between channel propagation in multiple-input multiple-output (MIMO) networks and geographical locations, and addressing both line-of-sight (LOS) and non-line-of-sight (NLOS) indoor conditions. In this paper, we propose an HMM-based framework that jointly characterizes the conditional propagation model and the evolution of the user trajectory. Specifically, the channel propagation in MIMO networks is modeled separately in terms of power, delay, and angle, with distinct models for LOS and NLOS conditions. The user trajectory is modeled using a Gaussian-Markov model. The parameters for channel propagation, the mobility model, and LOS/NLOS classification are optimized simultaneously. Experimental validation using simulated MIMO-Orthogonal Frequency-Division Multiplexing (OFDM) networks with a multi-antenna uniform linear arrays (ULA) configuration demonstrates that the proposed method achieves an average localization accuracy of 0.65 meters in an indoor environment, covering both LOS and NLOS regions. Moreover, the constructed radio map enables localization with a reduced error compared to conventional supervised methods, such as k -nearest neighbors (KNN), support vector machine (SVM), and deep neural network (DNN).

Index Terms—Radio map, trajectory recovery, LOS/NLOS classification, MIMO-OFDM networks

I. INTRODUCTION

The construction and utilization of radio maps have become a central focus in wireless communications and localization

The work was supported in part by Guangdong S&T Programme with Grant No. 2024B0101030002, the Basic Research Project No. HZQB-KCXYZ-2021067 of Hetao Shenzhen-HK S&T Cooperation Zone, the National Natural Science Foundation of China No. 62171398, the Shenzhen Science and Technology Program No. JCYJ20220530143804010 and No. KJZD20230923115104009, the Guangdong Basic and Applied Basic Research Foundation 2024A1515011206 and Research Projects No. 2017ZT07X152 and No. 2019CX01X104, the Shenzhen Outstanding Talents Training Fund 202002, the Guangdong Provincial Key Laboratory of Future Networks of Intelligence (Grant No. 2022B1212010001), and the Shenzhen Key Laboratory of Big Data and Artificial Intelligence (Grant No. ZDSYS201707251409055).

research [1]–[4]. A persistent challenge in radio map construction lies in the collection of location-labeled CSI data [5], which requires significant resources for drive testing and manual calibration. Radio maps establish crucial links between physical locations and channel characteristics, enabling innovative approaches for CSI acquisition, tracking, and prediction, as well as low-latency MIMO communications and environment-aware beamforming in mmWave massive MIMO systems [6, 7].

Traditional methods for radio map construction have proposed various strategies to reduce calibration efforts [8, 9]. For instance, [10] employed Kriging and covariance tapering techniques to construct radio maps in massive MIMO systems using a minimal amount of location-labeled CSI data. Similarly, [11] used sparse sampling and Bayesian learning inference to construct radio maps with limited location-labeled CSI data. However, these methods still necessitate calibration efforts to obtain even small amounts of location-labeled data. While some GPS-based methods [12] can provide location information, their performance is suboptimal in indoor environments and faces privacy access issues.

Channel charting emerges as an alternative paradigm, utilizing CSI embedding techniques to map high-dimensional channel data to low-dimensional latent spaces. Building on dimensionality reduction methods, subsequent work has explored various approaches such as autoencoders [13] and Sammon's mapping [14]. However, these methods still require a small amount of location labels, often rotating 2D or 3D data in the latent space based on limited location labels. Additionally, the latent space does not necessarily represent the physical world and does not account for dense multipath propagation in NLOS/LOS cross-environments [15]. Our prior work [16] employed a splitting-merging algorithm to recover trajectories but was limited to achieving only region-level accuracy.

In this paper, we propose a HMM-based framework that jointly characterizes the conditional propagation model and the evolution of user trajectories in MIMO networks. The model distinguishes between LOS and NLOS conditions, capturing the distinct channel propagation dynamics of each. The channel propagation in MIMO networks is separately modeled in terms of key parameters including power, delay, and angle, with distinct models for both LOS and NLOS environments. The mobile user's trajectory is modeled using

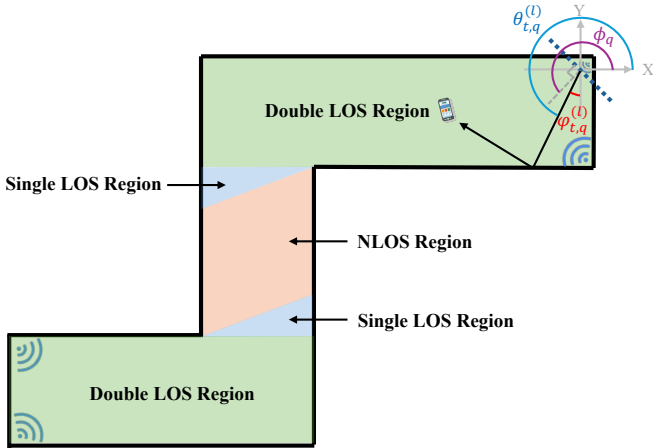


Figure 1. Schematic diagram of multipath signal emission angles and ULA antenna orientation.

a Gaussian-Markov model to capture the temporal-spatial relationship between each location and its preceding positions. The paper employs alternating optimization to jointly optimize the parameters for channel propagation, mobility models, and the classification of LOS/NLOS conditions.

The proposed method is validated through ray-tracing simulations conducted in MIMO-OFDM networks, covering both LOS and NLOS indoor environments. The results demonstrate that our method achieves an average localization error of 0.65 meters, significantly outperforming traditional angle- and power-based localization techniques, and also surpassing the performance of channel charting methods. Furthermore, by leveraging the constructed radio map, the method consistently achieves an average localization error below 1 meters, slightly outperforming conventional supervised approaches such as DNN, KNN, and SVM.

II. SYSTEM MODEL

A. Channel Model in MIMO-OFDM Networks

We consider a mobile user navigating an indoor environment with static obstructions, served by a network of Q access points (APs) located at known positions $\mathbf{o}_1, \mathbf{o}_2, \dots, \mathbf{o}_Q \in \mathbb{R}^2$. Each AP is equipped with a ULA consisting of N_t transmit antennas. The orientation angle $\phi_q \in [0, 2\pi)$ denotes the angle of the q -th AP's antenna array normal vector relative to the global coordinate system, as shown in Fig. 1. The system operates under a MIMO-OFDM framework with orthogonal subcarrier allocation.

The user trajectory is represented by a discrete sequence $\{\mathbf{x}_t\}_{t=1}^T \subset \mathbb{R}^2$ of T planar positions sampled at uniform time intervals. In the presence of multipath propagation, the frequency-selective channel between the q -th AP and the user at position \mathbf{x}_t consists of L resolvable paths. Each ℓ -th path ($\ell = 1, \dots, L$) is characterized by three parameters: the complex gain $\kappa_{t,q}^{(\ell)} \in \mathbb{C}$, the propagation delay $\tau_{t,q}^{(\ell)} \in \mathbb{R}_+$, and the angle of departure (AoD) $\theta_{t,q}^{(\ell)} \in [0, 2\pi)$. The effective

AoD in the q -th AP's local coordinate system is given by $\varphi_{t,q}^{(\ell)} = \theta_{t,q}^{(\ell)} - \phi_q$, where $\varphi_{t,q}^{(\ell)} \in (-\pi/2, \pi/2)$ due to the spatial aliasing limits of the ULA.

The normalized steering vector for the q -th AP's ULA at AoD θ is defined as:

$$\mathbf{a}_q(\theta) = \left[1, e^{-j\frac{2\pi}{\lambda}\Delta \sin \theta}, \dots, e^{-j\frac{2\pi}{\lambda}(N_t-1)\Delta \sin \theta} \right]^T, \quad (1)$$

where Δ denotes the inter-element spacing, $\lambda = c/f_c$ is the wavelength at the carrier frequency f_c , and $c = 3 \times 10^8$ m/s is the speed of light. The phase progression across array elements follows from the plane wave assumption in far-field radiation.

The channel for the q -th AP on the m -th subcarrier is given by $\mathbf{h}_{t,q}^{(m)} = \sum_{\ell=1}^L \kappa_{t,q}^{(\ell)} \cdot e^{-j2\pi \frac{m}{M} B \tau_{t,q}^{(\ell)}} \cdot \mathbf{a}(\varphi_{t,q}^{(\ell)})$, where B is the total bandwidth, M is the total number of subcarriers, and we assume $M > N_t$. $\varphi_{t,q}^{(\ell)}$ is the AoD relative to the antenna array's orientation ϕ_q , and $\mathbf{a}(\varphi_{t,q}^{(\ell)})$ is the steering vector of the ULA for the angle $\varphi_{t,q}^{(\ell)}$. The overall CSI is then formed by stacking the responses from each antenna $\mathbf{H}_{t,q} = [\mathbf{h}_{t,q}^{(1)}, \mathbf{h}_{t,q}^{(2)}, \dots, \mathbf{h}_{t,q}^{(M)}] \in \mathbb{C}^{N_t \times M}$. Here, the CSI $\mathbf{H}_{t,q}$ captures the frequency-selective multipath effects, delay spread, and spatiotemporal dynamics characteristic of wideband MIMO-OFDM channels.

B. Power-Angle-Delay Profile in LOS and NLOS Regions

The propagation environment is classified into two distinct regions: the LOS region $\mathcal{D}_0 \subset \mathbb{R}^4$ and the NLOS region $\mathcal{D}_1 \subset \mathbb{R}^4$. These regions are defined for each AP-user pair (\mathbf{o}, \mathbf{x}) , where \mathbf{o} represents the location of the AP and \mathbf{x} represents the user location. The regions satisfy the following condition:

$$\mathcal{D}_0 \cup \mathcal{D}_1 = \mathbb{R}^4, \quad \mathcal{D}_0 \cap \mathcal{D}_1 = \emptyset. \quad (2)$$

The radio map for each AP-user pair (\mathbf{o}, \mathbf{x}) is modeled as a piecewise function that distinguishes between LOS and NLOS propagation:

$$f(\mathbf{o}, \mathbf{x}; \mathcal{D}_0, \mathcal{D}_1) = \begin{cases} f_0(\mathbf{o}, \mathbf{x}), & \text{if } (\mathbf{o}, \mathbf{x}) \in \mathcal{D}_0, \\ f_1(\mathbf{o}, \mathbf{x}), & \text{if } (\mathbf{o}, \mathbf{x}) \in \mathcal{D}_1, \end{cases} \quad (3)$$

where $f_0(\mathbf{o}, \mathbf{x})$ and $f_1(\mathbf{o}, \mathbf{x})$ represent the propagation models for LOS and NLOS, respectively.

The radio map model decomposes the propagation environment into two complementary components: the geometric structure $\{\mathcal{D}_0, \mathcal{D}_1\}$ that characterizes the LOS and NLOS spatial domains, and the stochastic propagation model $\{f_0, f_1\}$ that governs signal attenuation and multipath phenomena. The geometric component $\mathcal{D}_k \subset \mathbb{R}^4$ for $k \in \{0, 1\}$ encodes obstacle-induced visibility constraints through spatial occupancy patterns of walls, furniture, and architectural features.

1) *Power Model with LOS/NLOS Discrimination:* The received signal strength (RSS) is estimated by the spatial-frequency domain power aggregation:

$$s_{t,q} = 10 \log_{10} \|\mathbf{H}_{t,q}\|_{\text{F}}^2, \quad (4)$$

where the CSI $\mathbf{H}_{t,q} \in \mathbb{C}^{N_t \times M}$ has elements $[H_{t,q}]_{(n,m)}$, and its squared Frobenius norm is given by $\|\mathbf{H}_{t,q}\|_F^2 = \sum_{n=1}^{N_t} \sum_{m=1}^M |[H_{t,q}]_{(n,m)}|^2$. Under Rayleigh fading assumptions, the complex channel coefficients $[H_{t,q}]_{(n,m)} \in \mathbb{C}$ for subcarrier $m \in \{1, \dots, M\}$ and antenna $n \in \{1, \dots, N_t\}$ are assumed to be independent and identically distributed (i.i.d.) complex Gaussian random variables.

In practical wireless systems, each AP operates in a unique environment, leading to variations in channel propagation due to obstacles, building materials, multipath effects, and antenna radiation patterns. Therefore, the RSS measurement is modeled by a conditional path loss model that accounts for the distinct propagation characteristics associated with different APs and environments $s_{t,q} = \beta_q^{(k)} - \alpha_q^{(k)} \log_{10} d(\mathbf{x}_t, \mathbf{o}_q) + \xi_q^{(k)}$, where $k \in \{0, 1\}$ indicates the propagation mode (LOS for $k = 0$ and NLOS for $k = 1$). The term $\xi_q^{(k)} \sim \mathcal{N}(0, \sigma_{s,q,k}^2)$ is to model the randomness due to multipath fading, body shadowing, and antenna pattern.

2) *Angle Model with LOS/NLOS Discrimination*: Consider the multipath propagation between the q -th AP and the mobile user at location \mathbf{x}_t . The frequency-domain CSI $\mathbf{H}_{t,q} \in \mathbb{C}^{N_t \times M}$ is observed over M OFDM subcarriers and N_t transmit antennas. The spatial covariance matrix is formulated as $\mathbf{R}_{t,q} = \frac{1}{M} \mathbf{H}_{t,q} \mathbf{H}_{t,q}^H \in \mathbb{C}^{N_t \times N_t}$, capturing the second-order statistics of the multipath channel. Through eigendecomposition, we obtain $\tilde{\mathbf{R}}_{t,q} = \tilde{\mathbf{u}}_{t,q}^{(1)} \lambda_1 (\tilde{\mathbf{u}}_{t,q}^{(1)})^H$, where $\tilde{\mathbf{u}}_{t,q}^{(1)}$ is the orthonormal eigenvector corresponding to the maximum eigenvalue λ_1 . The noise subspace matrix $\mathbf{U}_{t,q}$ is then constructed as $\mathbf{U}_{t,q} = [\tilde{\mathbf{u}}_{t,q}^{(2)}, \tilde{\mathbf{u}}_{t,q}^{(3)}, \dots, \tilde{\mathbf{u}}_{t,q}^{(N_t)}] \in \mathbb{C}^{N_t \times (N_t-1)}$, spanning the orthogonal complement of the signal subspace associated with the largest eigenvalue. Based on MUSIC algorithm, the AoD of the dominant path in the q -th AP coordinate system between the q -th AP and mobile user at location \mathbf{x}_t is estimated by:

$$\hat{\phi}_{t,q} = \underset{\varphi \in (-\pi/2, \pi/2)}{\operatorname{argmax}} \frac{1}{\mathbf{a}^H(\theta) \mathbf{U}_{t,q} \mathbf{U}_{t,q}^H \mathbf{a}(\varphi)}, \quad (5)$$

where $\mathbf{a}(\theta)$ is the steering vector given by (1). Thus, the AoD of the dominant path between the q -th AP and mobile user at location \mathbf{x}_t is estimated as $\hat{\theta}_{t,q} = \hat{\phi}_{t,q} + \phi_q$.

Assuming the AoD distribution follows a conditional LOS/NLOS Gaussian distribution $\hat{\theta}_{t,q} \sim \mathcal{N}(\phi(\mathbf{x}_t, \mathbf{o}_q), \sigma_{\theta,k}^2)$, $(\mathbf{o}_q, \mathbf{x}_t) \in \mathcal{D}_k$, where $\phi(\mathbf{x}_t, \mathbf{o}_q)$ defines the geometric azimuth angle between the user location \mathbf{x}_t and AP location \mathbf{o}_q . The variance $\sigma_{\theta,k}^2$ quantifies angular spread, which exhibits distinct behaviors in LOS ($k = 0$) and NLOS ($k = 1$) regimes. The NLOS variance $\sigma_{\theta,1}^2$ typically exceeds the LOS variance $\sigma_{\theta,0}^2$ due to multipath scattering in NLOS conditions.

3) *Delay Model with LOS/NLOS Discrimination*: Consider the channel $\mathbf{H}_{t,q}$ between the mobile user and the q -th AP at time slot t . The variance features are extracted as:

$$\nu_{t,q} = 10 \log_{10} \left(\operatorname{Var} \left(\left| \frac{\mathbf{H}_{t,q}}{\|\mathbf{H}_{t,q}\|_2} \right| \right) \right), \quad (6)$$

which quantifies multipath richness.

C. An HMM Formulation

Given the CSI $\mathbf{H}_{t,q}$, which can be separated as $\mathbf{y}_{t,q} = [s_{t,q}, \theta_{t,q}, \nu_{t,q}]^T$ using (4), (5) and (6), where $s_{t,q}$ represents the power, $\theta_{t,q}$ is the angle, and $\nu_{t,q}$ is the delay components. According to the power-angle-delay probability in Sec. II-B, we have the following probability density function:

$$p(\mathbf{y}_{t,q} | \mathbf{x}_t) = \begin{cases} \mathcal{N}(\boldsymbol{\mu}^{(0)}, \boldsymbol{\Sigma}^{(0)}), & (\mathbf{o}_q, \mathbf{x}_t) \in \mathcal{D}_0, \\ \mathcal{N}(\boldsymbol{\mu}^{(1)}, \boldsymbol{\Sigma}^{(1)}), & (\mathbf{o}_q, \mathbf{x}_t) \in \mathcal{D}_1. \end{cases} \quad (7)$$

where $\boldsymbol{\mu}^{(k)}(\mathbf{x}_t)$ is the mean vector for the k -th region (LOS or NLOS), defined as $\boldsymbol{\mu}^{(k)}(\mathbf{x}_t) = [\beta_q^{(k)} + \alpha_q^{(k)} \log_{10} d(\mathbf{o}_q, \mathbf{x}_t), \phi(\mathbf{x}_t, \mathbf{o}_q), b_k + a s_{t,q}]$, and the covariance matrix $\boldsymbol{\Sigma}^{(k)} = \operatorname{Diag}(\sigma_{s,q,k}^2, \sigma_{\theta,k}^2, \sigma_{\nu}^2)$.

Let $\mathcal{X}_t = (\mathbf{x}_1, \dots, \mathbf{x}_t)$ represent the trajectory of the user, and $\mathcal{H}_t = (\tilde{\mathbf{H}}_1, \tilde{\mathbf{H}}_2, \dots, \tilde{\mathbf{H}}_t)$ represent the accumulated channel measurements. Here, $\tilde{\mathbf{H}}_t = \{\mathbf{H}_{t,1}, \mathbf{H}_{t,2}, \dots, \mathbf{H}_{t,Q}\}$ denotes the set of all AP-side channels across subcarriers at time slot t . The goal is to recover the complete trajectory \mathcal{X}_T from the measurement history \mathcal{H}_T using Bayesian inference.

We adopt the Gauss-Markov model for user mobility dynamics \mathbf{x}_t . Let δ denote the slot duration. The movement at the t -th time slot is modeled as:

$$\mathbf{x}_t - \mathbf{x}_{t-1} = \gamma(\mathbf{x}_{t-1} - \mathbf{x}_{t-2}) + (1 - \gamma)\delta\bar{\mathbf{v}} + \sqrt{1 - \gamma^2}\delta\boldsymbol{\epsilon}, \quad (8)$$

where the temporal spacing between consecutive locations \mathbf{x}_{t-1} and \mathbf{x}_t is denoted as δ_t seconds, the velocity $(\mathbf{x}_t - \mathbf{x}_{t-1})/\delta$ at time slot t depends on the velocity from the previous time slot, following an auto-regressive model with parameter $0 < \gamma \leq 1$ and randomness $\boldsymbol{\epsilon} \sim \mathcal{N}(\mathbf{0}, \sigma_v^2 \mathbf{I})$. This captures the fact that acceleration is bounded in practice. The parameter $\bar{\mathbf{v}}$ models the average velocity. A higher γ value indicates stronger correlation between consecutive velocities, resulting in smoother movement. When $\gamma = 1$, the mobile user maintains a constant velocity.

The joint probability distribution decomposes through recursive application of Bayes' theorem, yields $p(\mathcal{H}_T, \mathcal{X}_T) = \prod_{t=1}^T p(\tilde{\mathbf{H}}_t | \mathbf{x}_t) \prod_{t=3}^T p(\mathbf{x}_t | \mathbf{x}_{t-1}, \mathbf{x}_{t-2})$, where $p(\tilde{\mathbf{H}}_t | \mathbf{x}_t)$ is given by (7) and $p(\mathbf{x}_t | \mathbf{x}_{t-1}, \mathbf{x}_{t-2})$ is given by (8).

Specifically, we consider the LOS/NLOS conditional spatial constrained, and the joint probability $p(\mathcal{H}_T, \mathcal{X}_T)$ can be written as:

$$\tilde{p}(\mathcal{H}_T, \mathcal{X}_T) = \prod_{t=1}^T \prod_{q=1}^Q \prod_{k=0}^1 p(\mathbf{y}_{t,q} | \mathbf{x}_t)^{u_{t,q}^{(k)}} \prod_{t=3}^T p(\mathbf{x}_t | \mathbf{x}_{t-1}, \mathbf{x}_{t-2}). \quad (9)$$

The logarithm of $\tilde{p}(\mathcal{H}_T, \mathcal{X}_T)$ can be written as:

$$\begin{aligned} \mathcal{L}(\mathcal{X}_T, \boldsymbol{\Theta}_p, \boldsymbol{\Theta}_m) = & \sum_{t=1}^T \sum_{q=1}^Q \sum_{k=0}^1 u_{t,q}^{(k)} \left\{ -\frac{1}{2} \left[(\mathbf{y}_{t,q} - \boldsymbol{\mu}^{(k)}(\mathbf{x}_t))^T \right. \right. \\ & \left. \left. (\boldsymbol{\Sigma}^{(k)})^{-1} (\mathbf{y}_{t,q} - \boldsymbol{\mu}^{(k)}(\mathbf{x}_t)) + \log |\boldsymbol{\Sigma}^{(k)}| + 3 \log(2\pi) \right] \right\} \\ & - \sum_{t=3}^T \left\{ \log[2\pi\sigma_v \sqrt{1 - \gamma^2}] \right\} \end{aligned}$$

$$+ \frac{\|\mathbf{x}_t - (1 + \gamma)\mathbf{x}_{t-1} + \gamma\mathbf{x}_{t-2} - (1 - \gamma)\delta\bar{\mathbf{v}}\|_2^2}{2(1 - \gamma^2)\delta^2\sigma_v^2} \Bigg\}$$

where $\Theta_p = \{\Phi_s, \Phi_\theta, \Phi_\nu, u_{t,q}^{(k)}\}$ represents the collection of propagation parameters. Here, $u_{t,q}^{(k)}$ is an auxiliary variable used to classify measurements into LOS or NLOS regions. The last term represents a constraint on the spatial structure.

Our goal is to maximize $\mathcal{L}(\mathcal{X}_T, \Theta_p, \Theta_m)$ with the LOS/NLOS classification constraint:

$$\begin{aligned} & \underset{\mathcal{X}_T, \Theta_p, \Theta_m}{\text{maximize}} \quad \mathcal{L}(\mathcal{X}_T, \Theta_p, \Theta_m) \\ & \text{subject to} \quad u_{t,q}^{(k)} \in \{0, 1\}, \quad u_{t,q}^{(0)} + u_{t,q}^{(1)} = 1. \end{aligned} \quad (10)$$

III. ALGORITHM

To solve the joint trajectory recovery and parameter estimation problem in equation (10), we observe that, given \mathcal{X}_T , the variables Θ_p and Θ_m are decoupled. This is because the first term in equation (10) only depends on Θ_p , while the second term only depends on Θ_m . Consequently, Θ_p and Θ_m can be solved through two parallel subproblems derived from equation (10), as follows:

$$\begin{aligned} (P1) : & \underset{\Theta_m}{\text{maximize}} \quad \sum_{t=3}^T \log p(\mathbf{x}_t | \mathbf{x}_{t-1}, \mathbf{x}_{t-2}, \Theta_m) \\ (P2) : & \underset{\Theta_p}{\text{maximize}} \quad \sum_{t=1}^T \sum_{q=1}^Q \sum_{k=0}^1 u_{t,q}^{(k)} \left[-\frac{1}{2} \left[(\mathbf{y}_{t,q} - \boldsymbol{\mu}^{(k)}(\mathbf{x}_t))^T (\boldsymbol{\Sigma}^{(k)})^{-1} (\mathbf{y}_{t,q} - \boldsymbol{\mu}^{(k)}(\mathbf{x}_t)) \right. \right. \\ & \quad \left. \left. + \log |\boldsymbol{\Sigma}^{(k)}| + 3 \log(2\pi) \right] \right] \\ & \text{subject to} \quad u_{t,q}^{(k)} \in \{0, 1\}, \quad u_{t,q}^{(0)} + u_{t,q}^{(1)} = 1. \end{aligned}$$

On the other hand, given the variables $\hat{\Theta}_p$ and $\hat{\Theta}_m$ as the solutions to (P1) and (P2), respectively, the trajectory \mathcal{X}_T can be solved by:

$$(P3) : \underset{\mathcal{X}_T}{\text{maximize}} \quad \mathcal{L}(\mathcal{X}_T, \Theta_p, \Theta_m)$$

This naturally leads to an alternating optimization strategy. In this strategy, we solve for \mathcal{X}_T from problem (P3), and then for $\hat{\Theta}_p$ and $\hat{\Theta}_m$ from problems (P1) and (P2) iteratively. Since the corresponding iterations never decrease the objective function in equation (10), which is bounded above, the iterations are guaranteed to converge.

The parameters $\{\bar{\mathbf{v}}, \sigma_v^2\}$ and $\{a_1^{(k)}, a_2^{(k)}\}$ in Θ_m are independent, and hence can be estimated separately. According to the mobility model in equation (8), the probability density function (PDF) of the location \mathbf{x}_t at time slot t is uniquely determined by the Karush–Kuhn–Tucker (KKT) conditions. Problem (P2) can be decomposed into three independent subproblems: (P2.1) with solution $\Phi_\nu, u_{t,q}^{(k)}$, (P2.2) with solution Φ_s , and (P2.3) with solution Φ_θ . To solve problem (P2.1), we adopt an iterative approach. Specifically, we first fix the binary variables $u_{t,q}^{(0)}$ and then optimize the parameters b_0, b_1, a , and σ_ν^2 .

For each fixed $u_{t,q}^{(0)}$, this becomes a linear regression problem. To solve for b_0, b_1 , and a , we apply the least squares method. The least squares problem for each class k is:

$$\underset{b_0, b_1, a}{\text{minimize}} \quad \sum_{t=1}^T \sum_{q=1}^Q u_{t,q}^{(k)} (\nu_{t,q} - b_k - a s_{t,q})^2$$

This is a weighted least squares problem, and the solution is obtained by solving for the parameters b_0, b_1 , and a . We define the matrix \mathbf{S}_k and the observation vector \mathbf{c}_k . Each row of \mathbf{S}_k corresponds to an input pair $(1, s_{t,1})$ and each entry of \mathbf{c}_k corresponds to the associated response $\nu_{t,1}$, for $t = 1, \dots, T$. The weighted least squares problem can be rewritten as:

$$\underset{b_k, a}{\text{minimize}} \quad \sum_{t=1}^T u_{t,q}^{(k)} (\mathbf{y}_t - \mathbf{S}_k [b_k, a]^T)^2$$

The least squares solution for the parameters $[b_k, a]^T$ is given by the normal equation:

$$[b_k, a]^T = (\mathbf{S}_k^T \mathbf{W}_k \mathbf{S}_k)^{-1} \mathbf{S}_k^T \mathbf{W}_k \mathbf{c}_k \quad (11)$$

where \mathbf{W}_k is the diagonal weighting matrix $\mathbf{W}_k = \text{diag}(u_{1,1}^{(k)}, u_{2,1}^{(k)}, \dots, u_{T,1}^{(k)})$.

To estimate the residual variance σ_ν^2 for each class k , we use the following formula:

$$\sigma_\nu^2 = \frac{1}{T} \sum_{t=1}^T \sum_{k=0}^1 u_{t,q}^{(k)} (\nu_{t,q} - b_k - a s_{t,q})^2 \quad (12)$$

Next, fix the parameters b_0, b_1, a , and σ_ν^2 , and optimize the binary variables $u_{t,q}^{(0)}$. The binary variables are updated using a classification method such as Maximum Likelihood Estimation (MLE) or Expectation-Maximization (EM). Thus, the binary indicator $u_{t,q}^{(k)}$ is updated by searching for $\max \exp\left(-\frac{(\nu_{t,q} - b_k - a s_{t,q})^2}{2\sigma_\nu^2}\right)$.

Repeat the alternative updating until convergence, thus solving problem (P2.1). In each iteration, the parameters b_0, b_1, a , and σ_ν^2 are updated by solving the least squares problem, and the binary variables $u_{t,q}^{(k)}$ are updated using the classification method. This alternating process continues until the algorithm converges, i.e., the updates to the parameters and binary variables no longer change significantly.

We solve problem (P2.2) using MLE by decomposing it into independent linear regression problems for each AP and set k . To solve problem (P2.3), we employ MLE by separately estimating the noise variances $\sigma_{\theta,0}^2$ and $\sigma_{\theta,1}^2$ by partitioning the data $\{(\theta_{t,q}, \phi(\mathbf{x}_t, \mathbf{o}_q))\}$ into subsets \mathcal{D}_0 and \mathcal{D}_1 using the indicator $u_{t,q}^{(k)}$. Here, \mathcal{D}_0 corresponds to $\sigma_{\theta,0}^2$ and \mathcal{D}_1 corresponds to $\sigma_{\theta,1}^2$.

Problem (P3) follows the classical HMM optimization form, with the distinction that the current state depends on the previous two states. It can be efficiently solved using a modified version of the Viterbi algorithm with a globally optimal guarantee.

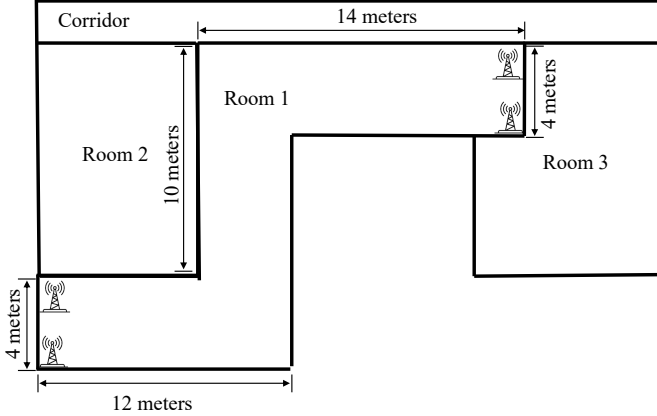


Figure 2. Simulated indoor environment with LOS and NLOS regions.

The overall algorithm is summarized as follows: First, the propagation parameters Θ_p and mobility parameters Θ_m are initialized randomly, and then the alternating update of \mathcal{X}_T , Θ_p , and Θ_m is performed iteratively until convergence.

IV. NUMERICAL EXPERIMENTS

We utilized Wireless Insite® to simulate an indoor environment with a 128 m^2 area. As illustrated in Figure 2, four APs with a height of 4 meters were manually deployed at the corners of the room. Each AP is equipped with an 8-antenna omnidirectional ULA array and configured with $M = 64$ subcarriers using a MIMO-OFDM model. The antenna orientation of each AP spans 180° , with a transmit power of 0 dBm. We set the antenna element spacing as $\Delta = 0.15 \text{ m}$, the carrier frequency as $f_c = 2.4 \text{ GHz}$, and the system bandwidth as $B = 20 \text{ MHz}$.

We recorded the CSI at receivers positioned at a height of 1.5 meters along predefined trajectories with lengths of 167 m, 160 m, and 240 m, corresponding to the training dataset, test dataset I, and test dataset II, respectively. The training dataset measurements were collected at walking speeds of 1, 1.5, 2, 2.5, 3, 3.5, and 4 m/s, with a sampling interval of $\delta = 0.2 \text{ s}$. The trajectory in the test dataset was generated by a random walk, with CSI measurements corrupted by zero-mean Gaussian noise of variance 0.2 and 0.4, respectively. We executed the proposed algorithm with a discretization resolution of $\tau = 0.1$

A. Trajectory Recovery Performance

The proposed algorithm achieves a LOS/NLOS classification accuracy of 98.5%. The trajectory estimation accuracy is quantified through the average localization error metric $E_{\text{loc}} = \frac{1}{T} \sum_{t=1}^T \|\mathbf{x}_t - \hat{\mathbf{x}}_t\|_2$, where $\mathbf{x}_t \in \mathbb{R}^2$ denotes the ground-truth position at time t , and $\hat{\mathbf{x}}_t$ represents the estimated coordinates from our algorithm. Comparative analysis employs four baseline methods, including: 1) Weighted Centroid Localization (WCL) [17] with position estimates $\hat{\mathbf{p}}_t = \sum_{q=1}^Q w_{t,q} \mathbf{o}_q$ where $w_{t,q} = 10^{s_{t,q}/20} / [\sum_{l=1}^Q 10^{s_{t,l}/20}]$, 2) POG-AMP [18]

Table I
COMPARISON OF AVERAGE LOCALIZATION ERROR (E_{loc}) ON THE TRAINING DATASET.

	WCL [17]	POG-AMP [18]	Channel Charting [19]	Proposed	GMA
NLOS	4.74	4.45	1.81	1.12	1.03
Single LOS	3.81	2.94	1.79	0.77	0.74
Double LOS	3.14	1.25	1.60	0.62	0.59
All	3.56	1.67	1.65	0.65	0.68

leverage periodic AoA measurements to estimated the user location. 3) Channel Charting [19] embeds CSI into real-world coordinates by introducing a bilateration loss and a line-of-sight bounding-box loss. 4) Genius-aided Map-Assisted (GMA) method that alternately updates mobility parameters and trajectory under known propagation models.

As shown in Table I, the proposed method achieves the best overall performance, with an average localization error of 0.65 meters. This result significantly outperforms the power-based WCL method [20], which yields an average error of 3.56 meters, as well as the angle-based POG-AMP approach [18] and the Channel Charting method [19], which report errors of 1.67 and 1.65 meters, respectively. Among these benchmarks, WCL performs poorly across all scenarios, especially under NLOS conditions where its error reaches 4.74 meters. POG-AMP shows strong performance in the Double LOS region with a low error of 1.25 meters, but suffers in NLOS environments where multipath-induced angular deviations severely degrade its accuracy, leading to a high error of 4.45 meters. Channel Charting demonstrates relatively stable performance across different LOS conditions, yet its lack of explicit delay modeling limits its achievable precision. In contrast, the superior accuracy of our proposed method stems from its integrated exploitation of power, angle, and delay information, enabling a more holistic characterization of the multipath propagation process. This joint modeling allows the system to better distinguish between LOS and NLOS scenarios and enhances localization robustness in complex environments. Although the proposed method's average error is marginally higher than that of GMA (0.68 meters), which represents the theoretical upper bound under perfect knowledge of propagation paths, the minimal difference of 0.03 meters underscores the near-optimality of our approach in practical settings.

B. Localization Performance

We evaluate the localization performance of the radio map using test datasets I and II, which have not been used for the radio map construction. A maximum-likelihood approach is used based on the conditional probability function, and the estimated location $\hat{\mathbf{x}}$ given the measurement vector \mathbf{y}_q is given by maximizing the propagation probability.

We compare the localization performance with the unsupervised method WCL [17]. For performance benchmarking, we also evaluate three supervised localization approaches KNN,

Table II
LOCALIZATION ERROR [METERS] ON THE TEST DATASET I AND II.

Method	Supervised			Unsupervised	
	KNN	SVM	DNN	WCL	Proposed
Test Dataset I	0.81	0.84	0.85	3.82	0.80
Test Dataset II	0.96	0.99	0.98	4.20	0.95

SVM [21], and DNN [22], which are trained using the training set with location labels that were not available to the proposed scheme. The parameters of baseline methods are determined and tuned using a ten-fold cross validation. For KNN, the optimal number of neighbors was found to be 8. A Gaussian kernel was used for SVM. For DNN, we adopt a three layer multilayer perceptron (MLP) neural network with 30 nodes in each layer to train the localization classifier.

Table II highlights three key findings based on rigorous experimental validation. First, the proposed unsupervised method significantly outperforms conventional unsupervised approaches, achieving an impressive reduction in mean localization error from 3.82 m to 0.80 m compared to WCL. Second, while the performance of the proposed method is comparable to that of supervised baselines, it enjoys the inherent advantage of being label-free. This superiority arises from the method's ability to accurately model signal characteristics and incorporate noise into the estimation process. As a result, it outperforms even supervised methods on the noisy Test Dataset I. Third, although all methods degrade on Test Dataset II due to increased signal noise, the proposed method exhibits better robustness to noise, leading to less performance degradation relative to other approaches.

V. CONCLUSION

This paper presents a novel unsupervised radio map construction method based on HMM-driven trajectory recovery in MIMO networks, effectively eliminating the need for location-labeled data calibration. By separately modeling channel propagation under both LOS and NLOS conditions and employing a Gaussian-Markov model to capture the spatial correlations in user trajectories, the proposed approach accurately recovers both propagation and mobility parameters through an alternating optimization framework. Experimental results validate the effectiveness of the method, achieving an average localization error of 0.65 meters, significantly outperforming traditional baseline approaches. Furthermore, localization performance based on the constructed radio map exhibits a slight reduction in error compared to conventional supervised methods, which can be attributed to the superior noise-handling capability of the proposed approach. Overall, this work offers a robust and scalable solution to reduce calibration costs and enhance localization accuracy in complex wireless environments.

REFERENCES

- [1] W. Liu and J. Chen, "UAV-aided radio map construction exploiting environment semantics," *IEEE Trans. Wirel. Commun.*, 2023.

- [2] R. Shrestha, D. Romero, and S. P. Chepuri, "Spectrum surveying: Active radio map estimation with autonomous uavs," *IEEE Trans. Wirel. Commun.*, vol. 22, no. 1, pp. 627–641, 2022.
- [3] H. Wang, J. Fang, H. Duan, and H. Li, "Compressive wideband spectrum sensing and signal recovery with unknown multipath channels," *IEEE Trans. Wirel. Commun.*, vol. 21, no. 7, pp. 5305–5316, 2022.
- [4] Z. Xing, H. Li, W. Liu, Z. Ren, J. Chen, J. Xu, and C. Qin, "Spectrum efficiency prediction for real-world 5G networks based on drive testing data," in *Proc. IEEE Wireless Commun. Netw. Conf. (WCNC)*, 2022, pp. 2136–2141.
- [5] Z. Xing and J. Chen, "Blind construction of angular power maps in massive MIMO networks," *IEEE Trans. Signal Process.*, vol. 00, no. 00, pp. 00–00, 2025.
- [6] D. Wu, Y. Zeng, S. Jin, and R. Zhang, "Environment-aware hybrid beamforming by leveraging channel knowledge map," *IEEE Trans. Wireless Commun.*, vol. 23, no. 5, pp. 4990–5005, 2024.
- [7] Z. Xing and J. Chen, "Constructing angular power maps in massive MIMO networks using measurements without location labels," in *Proc. IEEE Int. Conf. Commun. (ICC)*, vol. 0, 2025, pp. 0–0.
- [8] Z. Xing, J. Chen, and Y. Tang, "Integrated segmentation and subspace clustering for RSS-based localization under blind calibration," in *Proc. IEEE Global Commun. Conf. (GlobeCom)*, 2022, pp. 5360–5365.
- [9] Z. Xing and J. Chen, "HMM-based CSI embedding for trajectory recovery from RSS measurements of non-cooperative devices," in *Proc. IEEE Int. Conf. Acoust., Speech, Signal Process. (ICASSP)*, 2024, pp. 7060–7064.
- [10] W. B. Chikha, M. Masson, Z. Altman, and S. B. Jemaa, "Radio environment map based inter-cell interference coordination for massive-MIMO systems," *IEEE Trans. Mob. Comput.*, vol. 23, no. 1, pp. 785–796, 2022.
- [11] J. Wang, Q. Zhu, Z. Lin, J. Chen, G. Ding, Q. Wu, G. Gu, and Q. Gao, "Sparse bayesian learning-based hierarchical construction for 3D radio environment maps incorporating channel shadowing," *IEEE Trans. Wireless Commun.*, vol. 23, no. 10, pp. 14560–14574, 2024.
- [12] R. Whiton, "Cellular localization for autonomous driving: A function pull approach to safety-critical wireless localization," *IEEE Veh. Technol. Mag.*, vol. 17, no. 4, pp. 28–37, 2022.
- [13] P. Agostini, Z. Utkovski, and S. Stanczak, "Channel charting: An euclidean distance matrix completion perspective," in *Proc. IEEE Int. Conf. Acoust. Speech Signal Process.*, 2020, pp. 5010–5014.
- [14] P. Ferrand, A. Decurninge, L. G. Ordóñez, and M. Guillaud, "Triplet-based wireless channel charting: Architecture and experiments," *IEEE J. Sel. Areas Commun.*, vol. 39, no. 8, pp. 2361–2373, 2021.
- [15] Z. Xing, W. Liu, B. Li, J. Tian, M. Chu, and J. Chen, "HMM-based CSI embedding for trajectory recovery via feature engineering on MIMO-OFDM channels in LOS/NLOS regions," in *Proc. IEEE/CIC Int. Conf. Commun. China (ICCC) Workshops*, 2025, pp. 0–0.
- [16] Z. Xing and J. Chen, "Constructing indoor region-based radio map without location labels," *IEEE Trans. Signal Process.*, vol. 72, p. 2512–2526, 2024.
- [17] S. Phoemphon, C. So-In, and N. Leelathakul, "Fuzzy weighted centroid localization with virtual node approximation in wireless sensor networks," *IEEE Internet Things J.*, vol. 5, no. 6, pp. 4728–4752, 2018.
- [18] S. Wang, X. Jiang, and H. Wymeersch, "Cooperative localization in wireless sensor networks with aoa measurements," *IEEE Trans. Wirel. Commun.*, vol. 21, no. 8, pp. 6760–6773, 2022.
- [19] S. Taner, V. Palhares, and C. Studer, "Channel charting in real-world coordinates with distributed mimo," *IEEE Trans. Wirel. Commun.*, 2025.
- [20] K. Magowe, A. Giorgetti, S. Kandeepan, and X. Yu, "Accurate analysis of weighted centroid localization," *IEEE Trans. on Cognitive Commun. and Networking*, vol. 5, no. 1, pp. 153–164, 2018.
- [21] S. Sadowski, P. Spachos, and K. N. Plataniotis, "Memoryless techniques and wireless technologies for indoor localization with the internet of things," *IEEE Internet Things J.*, vol. 7, no. 11, pp. 10996–11005, 2020.
- [22] C.-Y. Chen, I. Alexander, C. Lai, P.-Y. Wu, and R.-B. Wu, "Optimization and evaluation of multidetector deep neural network for high-accuracy Wi-Fi fingerprint positioning," *IEEE Internet Things J.*, vol. 9, no. 16, pp. 15204–15214, 2022.